Anoyatis, G., Mylonakis, G., & Tsikas, A. (2019). An analytical continuum model for axially loaded end-bearing piles in inhomogeneous soil. *International Journal for Numerical and Analytical Methods in Geomechanics*, *43*(6), 1162-1183. https://doi.org/10.1002/nag.2886

Received 11 May 2018; | Revised 05 Nov 2018; | Accepted

DOI: xxx/xxxx

RESEARCH ARTICLE

An analytical continuum model for axially-loaded end-bearing piles in inhomogeneous soil

George Anoyatis*[1] | George Mylonakis[2] | Aggelos Tsikas[3]

[1]Civil & Environmental Engineering Division, University of the West of England, Bristol, UK
[2] Civil Engineering, University of Bristol, Bristol, UK; Civil Engineering, University of Patras, Patras, GR
[3] Research Engineering in Complex Energy Projects, Monogram AS, Oslo, Norway

Correspondence
*George Anoyatis
Email: george.anoyatis@uwe.ac.uk

Present Address
University of the West of England - UWE Bristol, Frenchay Campus, Coldharbour Lane, 3Q14A, Bristol, BS16 1QY, UK.

Summary

An approximate static solution is derived for the elastic settlement and load-transfer mechanism in axially loaded end-bearing piles in inhomogeneous soil obeying a power law variation in shear modulus with depth. The proposed generalised formulation can handle different types of soil inhomogeneity by employing pertinent eigen-expansions of the dependent variables over the vertical coordinate, in the form of static soil "modes", analogous to those used in structural dynamics. Contrary to available models for homogeneous soil, the associated Fourier coefficients are coupled, obtained as solutions to a set of simultaneous algebraic equations of equal rank to the number of modes considered. Closed-form solutions are derived for the: (i) pile head stiffness, (ii) pile settlement, axial stress, and side friction profiles leading to actual, depth-dependent, Winkler moduli, (iii) displacement and stress fields in the soil, (iv) average, depth-independent Winkler moduli to match pile head settlement. The predictive power of the model is verified via comparisons against finite-element analyses. The applicability to inhomogeneous soil of an existing regression formula for the average Winkler modulus is explored.

KEYWORDS:
piles, elasticity, analytical, Winkler, Tajimi, inhomogeneous

1 | INTRODUCTION

The analysis of pile settlement is a classical problem in geotechnical and piling engineering, which has attracted research interest for a long time. Relevant numerical approaches include finite-elements[1,2,3,4,5], Green's-functions and boundary element solutions[6,7,8,9,10,11], simplified t-z models[12,13,14,15], various hybrid formulations[16,17,18,19,20,21] and various reviews[22,23,24,25,26,27,28,29,30].

Despite the research and the publications, important aspects of the problem such as the effect of soil inhomogeneity, pile slenderness and pile-soil stiffness contrast on load transfer, remain poorly understood, mainly because of the lack of pertinent analytical tools, which can provide insight into the physics of pile-soil interaction. Indeed, most relevant analytical models are

restricted to two dimensions[31,32,23] and, therefore, cannot capture key aspects of the problem such as continuity of the medium in the vertical direction and attenuation of settlement with radial distance from the pile. On the other hand, three-dimensional analytical models which can provide more realistic predictions over two-dimensional counterparts have been explored to a lesser degree[33,34,35,36,37].

A promising family of three-dimensional analytical models is the one associated with the approximate continuum formulations of Matsuo & Ohara[38] and Tajimi[39], which, in turn, have their roots in the classical point-load solution of Westergaard[40]. These models (often referred to as *Tajimi* formulations) reduce the number of dependent variables by eliminating certain stress and displacement components in the governing equations and express the solution in terms of eigen-functions along the vertical coordinate. A number of closed form solutions for homogeneous soil have been obtained by means of this approach for piles[33,41,42,43,44,45,46] and retaining walls[47]. However, applications to inhomogeneous soil are very limited[48,49].

The static solution derived in this work extends the earlier studies by Nogami & Novak[33] and Mylonakis[36] to inhomogeneous soil with shear modulus obeying a power law variation with depth. As will be shown later in this article, handling an inhomogeneous medium is not straightforward, since special treatment is required to satisfy the boundary conditions at the pile-soil interface. The proposed generalised formulation can handle different types of soil inhomogeneity using natural soil "modes" and associated "eigenumbers" to describe the attenuation of soil displacement with depth and radial distance from the pile, respectively. These modes are similar to those used in structural dynamics and are derived under the more realistic assumption of zero radial stress and tangential strain[36]. The associated Fourier coefficients are now coupled and can be obtained as solutions to a set of simultaneous algebraic equations of rank equal to the number of modes considered.

Apart from its intrinsic theoretical interest, the proposed static model is advantageous over available two-dimensional models accounting for soil inhomogeneity[50,51] as it: (i) accounts for the continuity of the medium in both the horizontal and vertical directions; (ii) accounts for soil inhomogeneity in the vertical direction; (iii) accounts for pile-soil stiffness ratio, pile length to diameter ratio, and compressibility of the soil material;(iv) does not involve discretisation of the soil and the pile, nor does it employ empirical formulae or constants; (v) can be extended to cover more general situations such as simultaneous variation of material properties in the horizontal and vertical directions, soil anisotropy, poroelasticity, consolidation and dynamic response.

Additionally, the condition of zero stiffness at the soil surface (e.g., piles in sands), which is difficult to model numerically by discretising the soil medium into piecewise homogeneous regions, is also treated as a special case. Further, the proposed solution can provide a rational basis for developing a family of improved analytical models to assess other related problems in geotechnical engineering such as pile groups retaining walls and embedded circular foundations in non-homogeneous soils.

It is worth stressing that the proposed formulation is advantageous in several respects over pure numerical solutions as the latter require discretisation of the domain and/or the interfaces, and may encounter numerical difficulties in certain parameter ranges, as, for example, in the case of long compressible piles[52]. Also, these approaches are often limited by the analytical and

computational complexities associated with the underlying numerical procedures (particularly in three dimensions), which can make them unappealing to practising engineers.

The accuracy of the proposed static model is verified through comparisons with finite element analyses in terms of pile head stiffness for a variety of pile-soil configurations. Analytical solutions for end-bearing piles resting on a very hard bearing layer are derived for: (i) pile head stiffness, (ii) pile settlement, axial stress and side friction distributions with depth, (iii) actual, depth-dependent, Winkler modulus (ratio of side friction over corresponding settlement at the pile-soil interface), (iv) displacement and stress fields in the soil. In addition, a depth-independent (average) Winkler modulus that can be used in routine engineering calculations is obtained by matching the settlement at the pile head obtained from the proposed model and from a Winkler solution[23,30]. Also, an existing regression formula for an average Winkler modulus derived for homogeneous soils[36] is modified to account for soil inhomogeneity and results are found to be in good agreement with the proposed model.

2 | PROPOSED ANALYTICAL MODEL

The problem considered is illustrated in Figure 1 . A pile of length L and solid circular cross section of diameter d is embedded in a soil layer which rests on a rigid base. The pile is modelled as an elastic rod of Young's Modulus E_p and is subjected to a static axial head load P. Perfect contact (i.e., no gap nor slippage) is considered at the soil-pile interface. The soil layer of thickness H $(= L)$ is described by a constant Poisson's ratio ν_s and a depth-varying shear modulus $G_s(z)$ (z being the vertical coordinate) expressed by the following power-law function[53,54]

$$G_s(z) = G_{sH}\left[b + (1-b)\left(\frac{z}{H}\right)\right]^n \tag{1}$$

and

$$b = \left(\frac{G_{s0}}{G_{sH}}\right)^{1/n} \tag{2}$$

G_{sH} corresponds to the soil shear modulus at the base of the layer ($z = H$), and n and b are dimensionless inhomogeneity parameters. It is evident that $b = 0$ corresponds to zero stiffness at the soil surface, and $b = 1$ (or $n = 0$) to constant stiffness along the thickness of the layer (e.g., a heavily over-consolidated clay). Further, $n = 1$ corresponds to stiffness which varies linearly with depth, while the special case where $b = 0$ and $n = 1$ describes a Gibson[55] soil [i.e., $G_s(z) = G_{sH}(z/H)$]. A non-cemented sand may be approximated by setting $b = 0$ and $n = 1/2$. Note that, in the ensuing, except where specifically otherwise indicated, all numerical values are obtained using Poisson's ratio $\nu_s = 0.4$.

The mathematical analysis breaks into two modular problems: (i) analysis of the soil medium in presence of a cylindrical cavity (i.e. without the pile), and (ii) analysis of the pile as a rod inclusion.

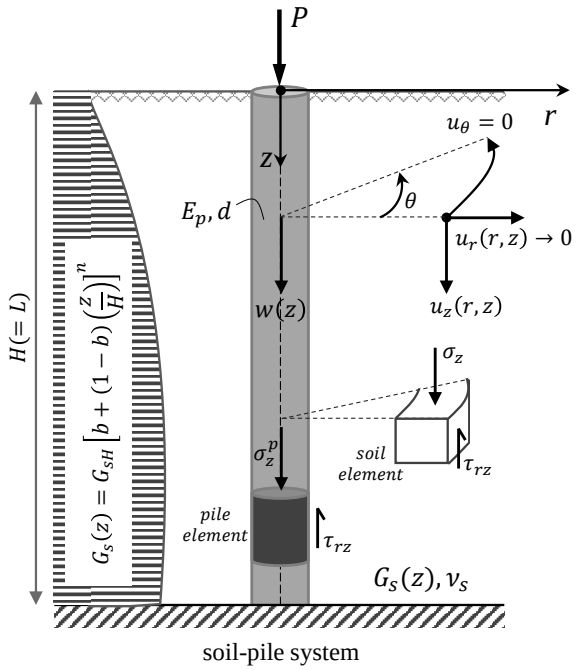

FIGURE 1 Problem considered: stresses and displacements in soil and pile.

2.1 | Soil Analysis

The equilibrium of vertical forces acting on a soil element in axisymmetric mode (Figure 1) yields the partial differential equation in terms of Cauchy stresses[31,36]

$$\frac{\partial(\tau\, r)}{\partial r} + r\,\frac{\partial \sigma}{\partial z} = 0 \tag{3}$$

where $\tau = \tau_{rz}(r,z)$ is the vertical shear stress, and $\sigma = \sigma_z(r,z)$ is the vertical normal stress. This formulation accounts for both axisymmetric shearing and compression of the soil surrounding the pile through the first and second term, respectively. The stress-displacement relations can be cast through the approximate equations[56]

$$\sigma \approx -\eta_s^2\, G_s(z)\,\frac{\partial u}{\partial z} \tag{4}$$

and

$$\tau \approx -G_s(z)\,\frac{\partial u}{\partial r} \tag{5}$$

where $u = u_z(r,z)$ is the vertical soil displacement and η_s is a dimensionless compressibility parameter which accounts, indirectly, for the effect of horizontal soil displacement u_r on soil stresses and depends solely on Poisson's ratio ν_s[36]

$$\eta_s = \sqrt{\frac{2}{1-\nu_s}} \tag{6}$$

Substituting Equations 4 and 5 into 3, the equilibrium equation is written in terms of displacements:

$$\frac{1}{r}\,\frac{\partial}{\partial r}\left(r\,\frac{\partial u}{\partial r}\right) \;+\; \eta_s^2\,\frac{\partial^2 u}{\partial z^2} \;+\; \eta_s^2\left[\frac{1}{G_s(z)}\,\frac{\partial G_s(z)}{\partial z}\right]\frac{\partial u}{\partial z} \;=\; 0 \tag{7}$$

The difference between Equation 7 and the corresponding expression in Mylonakis[36] for uniform soil lies in the presence of the third term in the left-hand side. Evidently, for a depth-independent G_s this term vanishes.

The solution to Equation 7 is obtained using the method of separation of variables. Expressing soil displacement as $u(r, z) = R(r)\,\Phi(z)$, where $R(r)$ and $\Phi(z)$ are solely functions of the spatial variables r and z, it is re-written as follows

$$\frac{1}{r}\,\frac{1}{R}\,\frac{d}{dr}\left(r\,\frac{dR}{dr}\right) \;+\; \eta_s^2\left[\frac{1}{G_s(z)}\,\frac{1}{\Phi}\,\frac{d}{dz}\left(G_s(z)\,\frac{d\Phi}{dz}\right)\right] \;=\; 0 \tag{8}$$

To ensure that the equality holds at every r and z, Equation 8 is decomposed into the pair of ordinary differential equations:

$$\frac{d^2R}{dr^2} \;+\; \frac{1}{r}\,\frac{dR}{dr} \;-\; q^2\,R \;=\; 0 \tag{9}$$

and

$$\frac{d}{dz}\left(\frac{G_s(z)}{G_{sH}}\,\frac{d\Phi}{dz}\right) \;+\; \alpha^2\left(\frac{G_s(z)}{G_{sH}}\right)\Phi \;=\; 0 \tag{10}$$

This method introduces real and positive parameters q and α which are linked through the compressibility coefficient η_s:

$$q \;=\; \eta_s\,\alpha \tag{11}$$

The solution is generated as the product of the solutions to Equations 9 and 10. Equation 9, admits the general solution

$$R(r) \;=\; A\,I_0(q\,r) \;+\; B\,K_0(q\,r) \tag{12}$$

where A and B are constants and $I_0(\,)$ and $K_0(\,)$ denote the modified Bessel functions of the zero order and the first and second kind, respectively. Considering bounded response at large radial distances from the pile, constant A must vanish; Equation 12 takes the simpler form:

$$R(r) \;=\; B\,K_0(q\,r) \tag{13}$$

Equation 10 is a Sturm-Liouville (SL) equation with variable coefficients and its solution depends on the functional form $G_s(z)$. Finding the distinct values a_m ($m = 1, 2, 3, \dots$) for which non-trivial solutions to satisfy the boundary conditions exist, is part of the SL theory. α_m's are referred to as the eigenvalues of the boundary-value problem and specific solutions to Equation 10 are the eigenfunctions $\Phi_m = \Phi_m(z)$ (i.e., soil modes). In this light, Equation 11 can be re-written as

$$q_m \;=\; \eta_s\,a_m \tag{14}$$

and the solution to Equation 7 can expressed in terms of infinite Fourier series

$$u(r,z) \;=\; \sum_{m=1}^{\infty} B_m \; K_0(q_m\, r)\; \Phi_m(z) \tag{15}$$

Likewise, shear stresses in the soil medium can be obtained from Equations 5 and 15

$$\tau(r,z) \;=\; \sum_{m=1}^{\infty} B_m \; q_m \; K_1(q_m\, r)\; G_s(z)\; \Phi_m(z) \tag{16}$$

where $K_1(\,)$ is the modified Bessel function of the first order and the second kind.

To evaluate u and τ the Fourier coefficients B_m are required, which can be obtained by imposing the compatibility of displacements at the pile-soil interface.

Orthogonality of soil modes

Fundamental to the herein reported model is the implementation of the orthogonality identity of the soil modes:

$$\int_0^H G_s(z)\; \Phi_m(z)\; \Phi_k(z)\; dz \;=\; 0, \quad for \quad m \neq k \tag{17}$$

where $k \;=\; 1, 2, 3, \ldots$ is a dummy variable. In Sturm-Liouville theory $G_s(z)$ is a weight function and the associated eigenfunctions Φ are orthogonal with respect to it [57]. This is valid for existing solutions in homogeneous soils [33,36,44], where the orthogonality of the soil modes is expressed in the simpler form $\int_0^H \Phi_m\, \Phi_k\, dz = 0$ (for $m \neq k$) as G_s is depth-independent and escapes the integration.

2.2 | Pile analysis

In the realm of strength-of-materials theory the equilibrium of vertical forces acting on a pile segment yields [36]

$$-\, E_p\, A_p\, \frac{\partial^2 \mathrm{w}}{\partial z^2} \;+\; \pi\, d\, \tau_0 \;=\; F(z) \tag{18}$$

where A_p is the pile cross sectional area and $\tau_0 = \tau(d/2, z)$ (Equation 16) is the profile of vertical soil reaction at the soil-pile interface (side friction). $F(z) = P\, \delta(z)$ represent the load P at the pile head in the form of distributed body forces [$\delta(z)$ being the familiar delta (Dirac) distribution] and can be expanded into Fourier series as:

$$P\; \delta(z) \;=\; \sum_{m=1}^{\infty} F_m\; G_s(z)\; \Phi_m(z) \tag{19}$$

The coefficients F_m can be determined by multiplying both sides of the equation by $G_s(z)\Phi_k(z)$ integrating over the soil thickness H and applying the orthogonality identity of Equation 17

$$F_m = \frac{\int_0^H P\delta(z)\Phi_m(z)dz}{\int_0^H G_s(z)\Phi_m^2(z)dz} = P\frac{\int_0^H \Phi_m(0)dz}{\int_0^H G_s(z)\Phi_m^2(z)dz} \tag{20}$$

Considering perfect contact at the pile-soil interface [i.e., $w(z) = u(d/2, z)$] and substituting equations (12), (13) and (16) into (15), the pile equilibrium equation is re-written as

$$-E_p A_p \sum_{m=1}^{\infty} B_m K_0(s_m)\Phi_m''(z) + 2\pi \sum_{m=1}^{\infty} B_m s_m K_1(s_m) G_s(z)\Phi_m(z) = \sum_{m=1}^{\infty} F_m G_s(z)\Phi_m(z) \tag{21}$$

where $\Phi_m''(z)$ is the second derivative of soil modes Φ_m with respect to the z and $s_m = a_m \eta_s d/2$. Key to determining the unknown parameters B_m is removing the infinite sums from Equation 21 and requiring equality to hold for each term individually. Accordingly, the presence of product $G_s(z)\Phi_m(z)$ in all terms is required to apply the orthogonality identity.

To comply with the above requirement, function $\Phi_m''(z)$ is expanded over the vertical coordinate in a manner analogous to Equation 19

$$\Phi_m''(z) = \sum_{j=1}^{\infty} S_j G_s(z)\Phi_j(z) \tag{22}$$

where $j = 1, 2, 3, \ldots$ is a new dummy variable. The associated coefficients S_j can be determined using the orthogonality identity of the soil modes

$$S_j = \frac{\int_0^H \Phi_m''(z)\Phi_j(z)dz}{\int_0^H G_s(z)\Phi_j^2(z)dz} = -\frac{\int_0^H \Phi_m'(z)\Phi_j'(z)dz}{\int_0^H G_s(z)\Phi_j^2(z)dz} \tag{23}$$

which makes use of the boundary conditions $\Phi'(0) = 0$ and $\Phi(H) = 0$. Substituting Equation 22 in 21 yields

$$-E_p A_p \sum_{m=1}^{\infty} B_m K_0(s_m)\left(\sum_{j=1}^{\infty} S_j G_s(z)\Phi_j(z)\right) + 2\pi \sum_{m=1}^{\infty} B_m s_m K_1(s_m) G_s(z)\Phi_m(z) = \sum_{m=1}^{\infty} F_m G_s(z)\Phi_m(z) \tag{24}$$

Multiplying Equation 24 by Φ_k, integrating with respect to z in the interval $(0, H)$ and considering the orthogonality identity yields

$$-E_p A_p \sum_{m=1}^{\infty} B_m K_0(s_m)\left(S_k \int_0^H G_s(z)\Phi_k^2(z)\,dz\right) + 2\pi \sum_{k=1}^{\infty} B_k s_k K_1(s_k)\left(\int_0^H G_s(z)\Phi_k^2(z)\,dz\right) = \sum_{k=1}^{\infty} F_k\left(\int_0^H G_s(z)\Phi_k^2(z)\,dz\right) \tag{25}$$

in which, assuming uniform convergence, an interchange between the summation and integration signs in all terms has been applied. Note that orthogonality results in $j = k$ and $m = k$ to attain non-zero integrals. Further, substituting Equations 20 and

23 into 25, yields for every term k:

$$E_p\,A_p\sum_{m=1}^{\infty}B_m\,K_0(s_m)\left(\int_0^H\Phi_m^{'}(z)\,\Phi_k^{'}(z)\,dz\right)\;+\;2\,\pi\,B_k\,s_k\,K_1(s_k)\left(\int_0^H G_s(z)\,\Phi_k^2(z)\,dz\right)\;=\;P\,\Phi_k(0) \tag{26}$$

Re-arranging Equation 26 in a matrix form, B_m values can be obtained from the solution of a set of simultaneous algebraic equations:

$$[R_{km}]\,\{B_m\}\;=\;P\,\{\Phi_k(0)\} \tag{27}$$

where B_m and Φ_k are vectors of length k, $k = 1, 2, 3, \ldots N$, $m = 1, 2, 3, \ldots N$, N is the number of "modes" considered in the analysis and $[R_{km}]^{-1}$ is the inverse of the square stiffness matrix R_{km}

$$R_{km}\;=\;E_p\,A_p\,K_0(s_m)\left(\int_0^H\Phi_m^{'}(z)\,\Phi_k^{'}(z)\,dz\right)\;+\;\left[2\,\pi\,s_k\,K_1(s_k)\left(\int_0^H G_s(z)\,\Phi_k^2(z)\,dz\right)\right]\delta_{km} \tag{28}$$

In Equation 28 the terms related to Kronecker delta δ_{km} are added only to the diagonal terms of the matrix R_{km} [$\delta_{km} = 0$ for $k \neq m$ and $\delta_{km} = 1$ for $k = m$].

Solutions for piles in a homogeneous soil[33,36,44], generate coefficients B_m independently (note that in that case matrix R_{km} in Equation 27 is diagonal), whereas herein, B_m's are coupled (Equation 27).

Taking into account perfect bonding at the soil-pile interface [i.e., $\mathrm{w}(z) = u(d/2, z)$], pile displacement can be determined from Equation 15:

$$\mathrm{w}(z)\;=\;\sum_{m=1}^{N}B_m\,K_0(s_m)\,\Phi_m(z) \tag{29}$$

The axial stresses σ^p acting in the pile are determined by differentiating Equation 29 with respect to the spatial variable z [$= E_p\,\mathrm{w}^{'}(z)$]:

$$\sigma^p(z)\;=\;E_p\sum_{m=1}^{N}B_m\,K_0(s_m)\,\Phi_m^{'}(z) \tag{30}$$

where $\Phi_m^{'}$ is the first derivative of function Φ_m ($d\Phi_m/dz$). An equivalent expression to Equation 30 can be obtained from manipulating the equilibrium Equation 18:

$$\sigma^p(z)\;=\;\left(P\;-\;\pi\,d\int_0^z\tau_0\;dz\right)/A_p \tag{31}$$

The above alternative is advantageous over Equation 30 as the integration instead of the differentiation with respect to the spatial variable z improves convergence even for a small number of modes. Numerical results for σ^p shown later in this work are obtained from Equation 31.

3 | STATIC SOIL MODES

The general solution to Equation 10 as well as its first derivative are obtained from the following expressions:

$$\Phi(z) \;=\; \left(\frac{1-b}{\alpha}\,A(z)\right)^{(1-n)/2}\left[C\,J_{(n-1)/2}\Big(A(z)\Big) \;+\; D\,Y_{(n-1)/2}\Big(A(z)\Big)\right] \tag{32}$$

and

$$\Phi'(z) \;=\; -\,\alpha\left(\frac{1-b}{\alpha}\,A(z)\right)^{(1-n)/2}\left[C\,J_{(n+1)/2}\Big(A(z)\Big) \;+\; D\,Y_{(n+1)/2}\Big(A(z)\Big)\right] \tag{33}$$

In the above equations, C and D are constants to be determined from the boundary conditions, $J(\,)$ and $Y(\,)$ are the Bessel functions of the first and second kind, respectively, and $A(z)$ is a dimensionless parameter (argument of the Bessel functions) given from the expressions below:

$$A(z) \;=\; \frac{\alpha\,H}{1-b}\left[b \;+\; (1-b)\left(\frac{z}{H}\right)\right] \tag{34}$$

Considering the boundary conditions of zero displacements at the base of the soil layer and zero normal stresses at the soil surface, Equations 32 and 33 yield, respectively:

$$C\,J_{(n-1)/2}\big(A_H\big) \;+\; D\,Y_{(n-1)/2}\big(A_H\big) \;=\; 0 \tag{35}$$

and

$$C\,J_{(n+1)/2}\big(A_0\big) \;+\; D\,Y_{(n+1)/2}\big(A_0\big) \;=\; 0 \tag{36}$$

where $A_H = A(z = H)$ and $A_0 = A(z = 0)$. To allow for non-trivial solutions, the determinant of the matrix formed by the pair of Equations 35 and 36 must be zero. This constraint yields the following characteristic equation

$$J_{(n+1)/2}\big(A_0\big)\,Y_{(n-1)/2}\big(A_H\big) \;+\; J_{(n-1)/2}\big(A_H\big)\,Y_{(n+1)/2}\big(A_0\big) \;=\; 0 \tag{37}$$

Its roots α are the desired eigenvalues α_m ($m = 1, 2, 3, \dots$). Expressing constant D as a function of constant C using Equation 35, Φ and associated derivatives Φ' can be cast in the forms:

$$\Phi_m(z) \;=\; C\left(\frac{1-b}{\alpha_m}\,A(z)\right)^{(1-n)/2}\left[J_{(n-1)/2}\Big(A(z)\Big) \;-\; \frac{J_{(n-1)/2}\big(A_H\big)}{Y_{(n-1)/2}\big(A_H\big)}\,Y_{(n-1)/2}\Big(A(z)\Big)\right] \tag{38}$$

and

$$\Phi'(z) \;=\; -\,C\,\alpha_m\left(\frac{1-b}{\alpha_m}\,A(z)\right)^{(1-n)/2}\left[J_{(n+1)/2}\Big(A(z)\Big) \;-\; \frac{J_{(n-1)/2}\big(A_H\big)}{Y_{(n-1)/2}\big(A_H\big)}\,Y_{(n+1)/2}\Big(A(z)\Big)\right] \tag{39}$$

For the special case of a soil with zero stiffness at the surface ($b = 0$), the condition of a stress-free soil surface requires setting $D = 0$. Thus, Equations 37, 38 and 39 take the simpler forms (C being a new integration constant):

$$J_{(n+1)/2}\big(\alpha_m H\big) \;=\; 0 \tag{40}$$

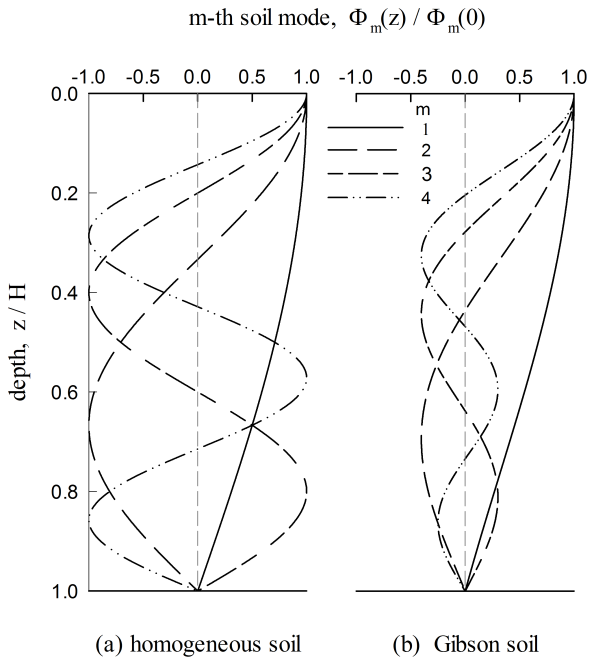

FIGURE 2 Static soil modes for a homogeneous and a Gibson soil ($b = 0$ and $n = 1$, Equations 1 and 2).

$$\Phi_m(z) = C\, z^{(1-n)/2}\, J_{(n-1)/2}\left(\alpha_m z\right) \tag{41}$$

$$\Phi'_m(z) = -C\, \alpha_m\, z^{(1-n)/2}\, J_{(n+1)/2}\left(\alpha_m z\right) \tag{42}$$

Equation 38 fits in Equations 15 and 29, while Equation 39 fits in 16 and 30 and constant C is absorbed into constant B_m (which is calculated via Equation 27). Solutions to Equation 40 have been studied extensively and are available in tabulated form[58].

The first four mode shapes (i.e., Φ_1, Φ_2, Φ_3, Φ_4) for a homogeneous and a Gibson soil are illustrated in Figure 2 . Evidently, the difference between the mode shapes in the two media is more pronounced for higher modes. Additional results are presented in Figure 3 , where zero stiffness at the surface ($b = 0$) is considered. Each mode is normalized to be unitary at the pile head and is plotted separately for different values of the inhomogeneity parameter n. For the first mode all curves practically collapse into a single one. The effect of inhomogeneity is pronounced for higher modes via gradually stronger peaks and troughs of the cosine-like curves. It is noteworthy that contrary to structural dynamics where the first mode often dominates response, a much higher number of modes must be used in this method - probably because of the dissimilarity of the shapes Φ_m to a delta function. The sufficient number of modes is discussed in the following section.

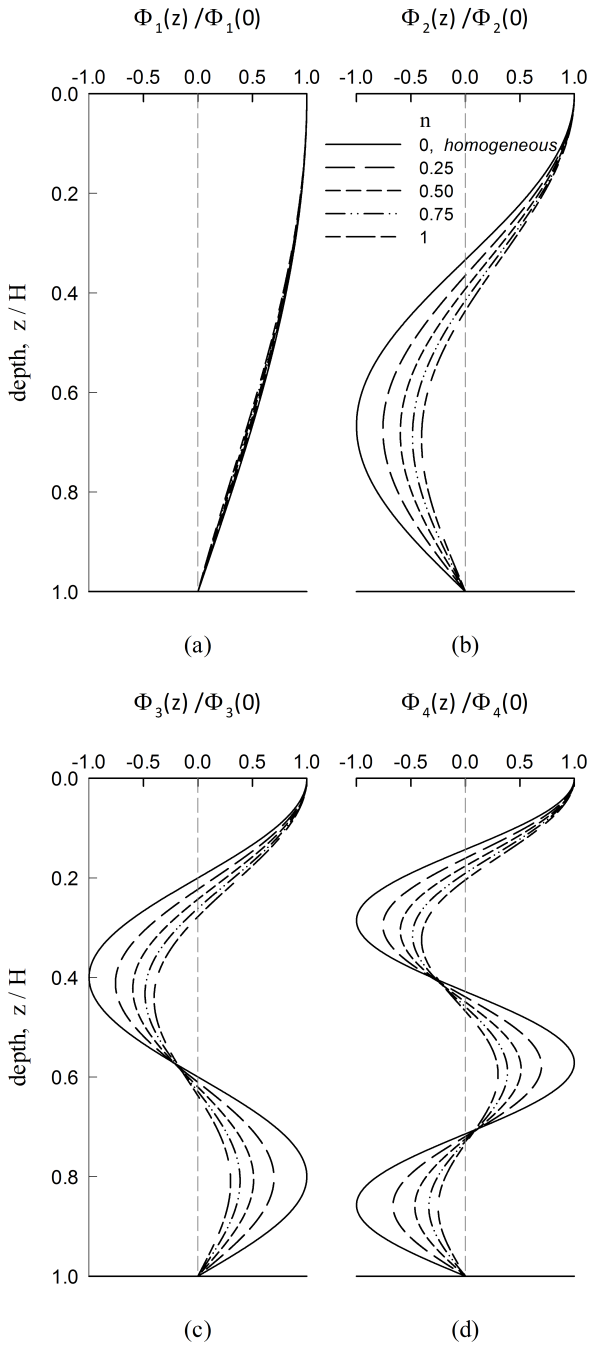

FIGURE 3 Effect of inhomogeneity on the first four static soil modes for a soil with zero stiffness at its surface ($b = 0$, Equation 2).

4 | MODEL VERIFICATION

Table 1 presents pile head stiffness K (load P over settlement w_0 at the pile head) obtained from the proposed model using different number of modes.

$$K = \frac{P}{w_0} = \frac{P}{\sum_{m=1}^{\infty} B_m \, K_0(s_m) \, \Phi_m(0)} \tag{43}$$

TABLE 1 Normalised pile head stiffness $K/E_{sH}\,d$: effect of number of modes (Equation 43) and comparison against results obtained from rigorous finite element (FE) analyses by means of the commercial software ANSYS[59] for various soil-pile configurations. Soil: $\nu_s = 0.4$, $b = 0$, $n = 0.5$; Pile Poisson's ratio $\nu_p = 0.2$.

		Normalised Pile Head Stiffness $K/E_{sH}d$								
		FE (F)	**Proposed model** (P) (P) Number of modes N				Discrepancy (%) $(P-F/F)\times 100\%$ Number of modes N			
E_p/E_{sH}	L/d	**FE** (F)	10	20	500	1000	10	20	500	1000
100	15	7.168	7.347	7.264	7.248	7.246	2.5	1.3	1.1	1.1
100	25	5.489	5.678	5.596	5.580	5.578	3.4	1.9	1.7	1.6
100	50	4.326	4.544	4.438	4.418	4.416	5.0	2.6	2.1	2.1
100	100	3.623	3.888	3.734	3.706	3.702	7.3	3.1	2.3	2.2
300	15	17.784	18.084	17.916	17.883	17.880	1.7	0.7	0.6	0.5
300	25	12.144	12.417	12.285	12.258	12.255	2.2	1.2	0.9	0.9
300	50	8.430	8.709	8.580	8.553	8.550	3.3	1.8	1.5	1.4
300	100	6.768	7.089	6.918	6.885	6.882	4.7	2.2	1.7	1.7
1000	15	54.470	55.180	54.710	54.620	54.610	1.3	0.4	0.3	0.3
1000	25	34.320	34.820	34.510	34.450	34.440	1.5	0.6	0.4	0.3
1000	50	20.110	20.530	20.310	20.270	20.260	2.1	1.0	0.8	0.7
1000	100	14.070	14.490	14.280	14.230	14.220	3.0	1.5	1.1	1.1

Results in terms of normalised stiffness $K/E_{sH}\,d$, are compared against results from the finite-element code ANSYS[59] using soil and pile Poisson's ratios $\nu_s = 0.4$ and $\nu_p = 0.2$, respectively, and approximately 10^3 elements in axisymmetric mode. The predictions are very good over a wide range of geometries ($L/d = 15$ to 100) and pile-soil stiffness ratios ($E_p/E_{sH} = 100$ to 1000), with minimum and maximum deviation from the rigorous solution being 0.3% (for short, stiff piles) and 7.3% (for long, soft piles), respectively. Evidently, using 10^3 modes, the discrepancy does not exceed 2.2%. Comparisons further indicate that the shorter and stiffer the pile, the better is the performance of the model for a given number of modes. More modes are required for long piles in stiff soil and less modes for short piles in soft soil. Naturally, a higher number of modes leads to improved predictions in all cases.

Further comparisons with the solution of Novak and Sharnouby[60] are presented in Figure 4 . While results for floating or friction piles are available in the literature[61,10,62], studies for end-bearing piles (i.e., fixed tip piles) in vertically inhomogeneous soils are very limited. Herein, results are presented in terms of a normalized stiffness parameter $f_{v1} = \frac{R}{E_p A_p} K$ (Eq. 8a,[60]), where R is the pile radius. A broad range of pile geometries in a very soft soil (E_p/G_{sH}) are investigated and results are found to be in excellent agreement. Note that the Novak and Sharnouby values are obtained from a dynamic analysis where the familiar dimensionless frequency $a_0 = \frac{\omega R}{V_s} = 0.3$. Since the stiffnesses of the single piles examined in Figure 4 are expected to vary weakly with frequency, these results are considered comparable.

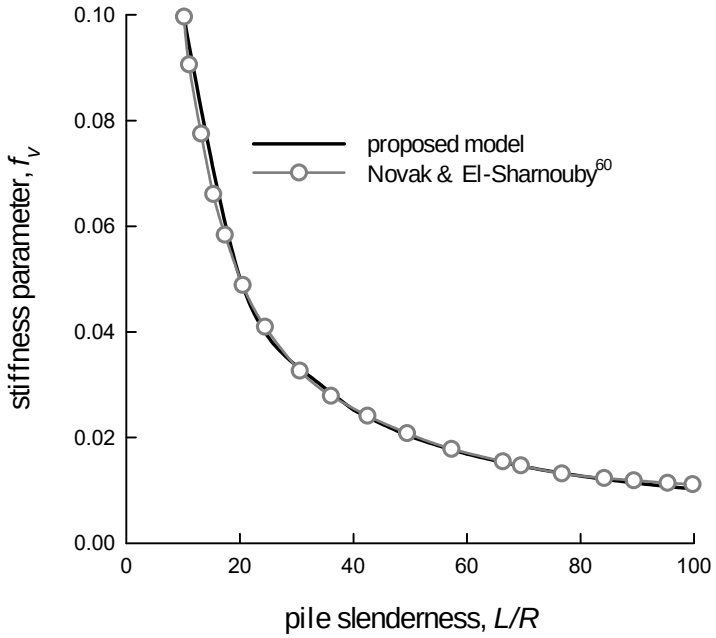

FIGURE 4 Variation of the stiffness parameter f_{v1} with pile slenderness L/R (R = pile radius) for a soil with $E_p/G_{sH} = 10000$ zero stiffness at its surface ($b = 0$, Equation 2) and parabolic variation of stiffness with depth ($n = 2$, Equation 1). Proposed results using $N = 100$ number of modes are compared against result from the solution of Novak and El-Sharnouby[60].

Pile head stiffness

Additional results for pile head stiffness, in terms of $K/E_p d$, using $N = 10^2$ modes are presented in Figures 5 and 6 . For piles in a soil with zero stiffness at the surface (Figure 5), stiffness drops with increasing pile slenderness L/d (the attenuation being stronger for small L/d's) and inhomogeneity n. The effect of inhomogeneity is stronger for low pile-soil stiffness ratios and diminishes with increasing stiffness contrast, as pile tip resistance gradually becomes more significant than side friction. For piles in a soil with finite stiffness at the surface (Figure 6) stiffness $K/E_p d$ increases with increasing G_{s0}/G_{sH} under constant values of n and E_p/E_{sH}. This trend is stronger for stiff soil ($E_p/E_{sH} = 100$), as the soil component gradually dominates the

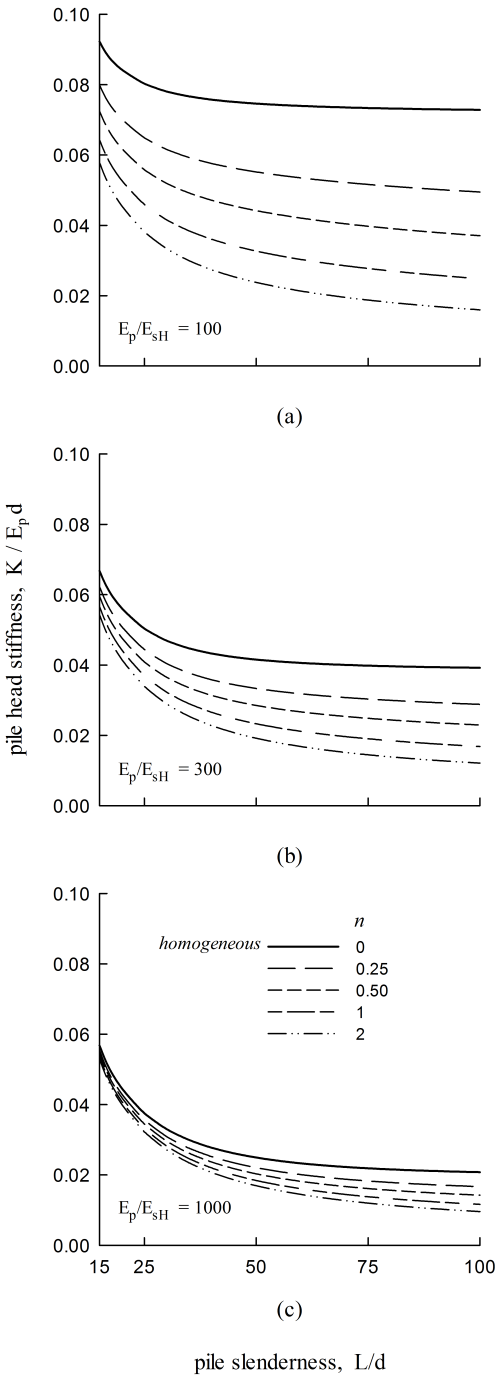

FIGURE 5 Variation of pile head stiffness with pile slenderness for selected values of the inhomogeneity parameter n and the pile-soil stiffness ratio E_p/E_{sH}, for a soil with zero stiffness at its surface($b = 0$, Equation 2). Number of modes used $N = 500$.

system's behaviour. Like in Figure 6 , head stiffness for piles in homogeneous soils always attain the highest values. As a general pattern, high values of pile-soil stiffness contrast tend to supress the influence of soil inhomogeneity (Figure 6 (c)).

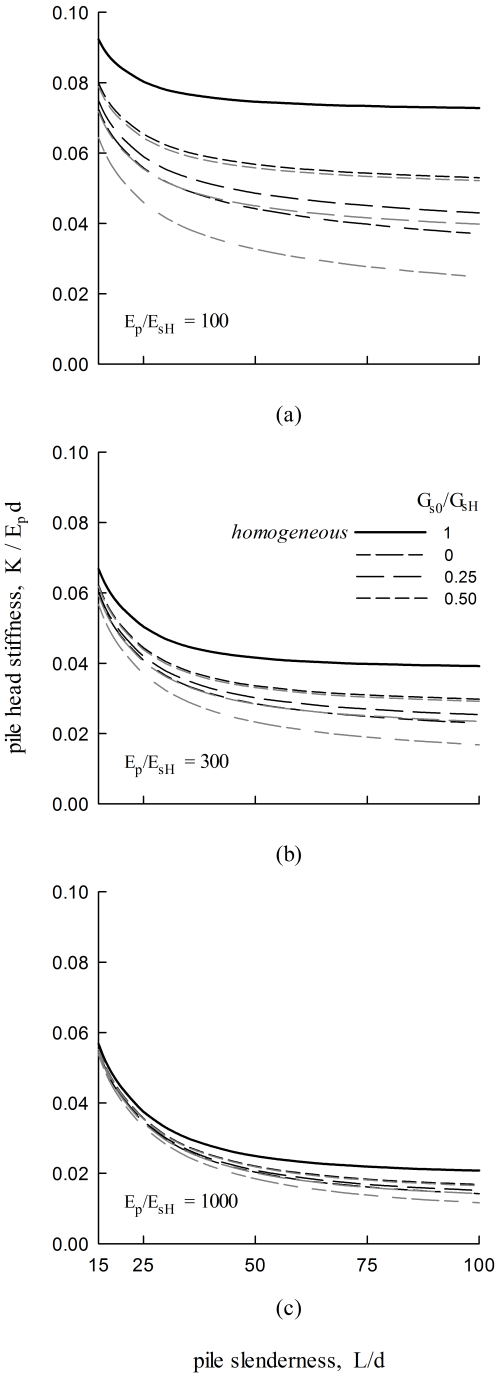

FIGURE 6 Variation of pile head stiffness with pile slenderness for selected values of inhomogeneity parameters n and b, and pile-soil stiffness ratio E_p/E_{sH}. The black curves refer to $n = 0.5$ and the grey curves to $n = 1$. Number of modes used $N = 500$.

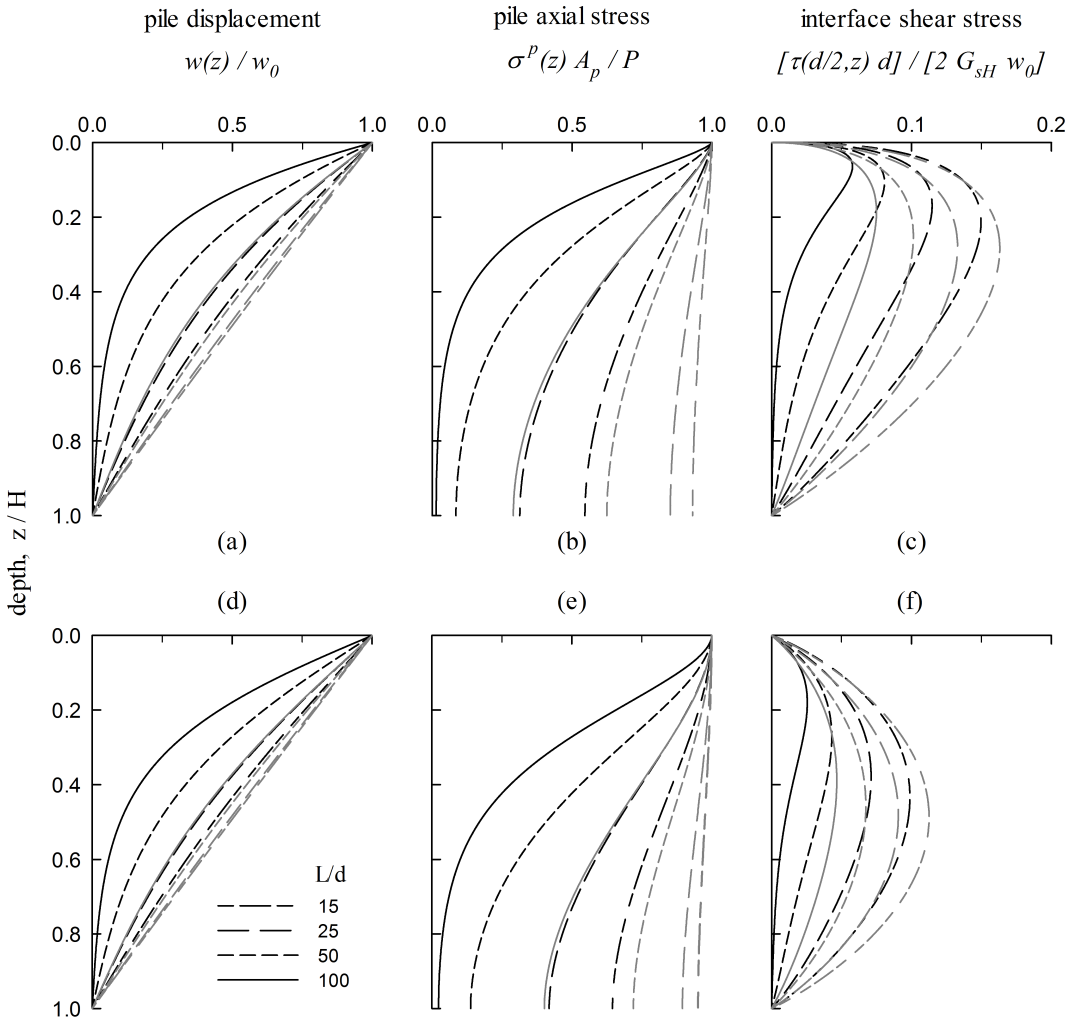

FIGURE 7 Profiles of pile displacement, vertical pile normal stresses and shear stresses at the pile-soil interface for different geometries of piles embedded in soils with zero stiffness at their surface ($b = 0$, Equation 2). The black curves refer to $E_p/E_{sH} = 100$ and the grey curves to $E_p/E_{sH} = 1000$. Sub-figures $(a) - (c)$ correspond to $n = 0.5$ and sub-figures $(d) - (f)$ to $n = 1$. Number of modes used $N = 1500$.

5 | NUMERICAL RESULTS

The variations with depth of normalised pile displacement, pile axial stresses and vertical shear tractions at the pile-soil interface (side friction) are shown in Figures 7 , 8 and 9 . Results are presented for different pile geometries and degrees of inhomogeneity. Figure 7 shows that the attenuation of settlement with depth is stronger for longer piles (e.g., $L/d = 100$) and stiffer soil (e.g., $E_p/E_{sH} = 100$) (Figure 7 (a)). The same trend (supressed though) is observed when increasing levels of inhomogeneity (Figure 7 (d)). Short piles ($L/d = 15$) exhibit a column-like behaviour regardless of pile- soil stiffness ratio, as evident in the settlement graphs 7 (a) and 7 (d). In the same figure, pile axial stresses (Figures 7 (b), 7 (e)) attain their maxima at the

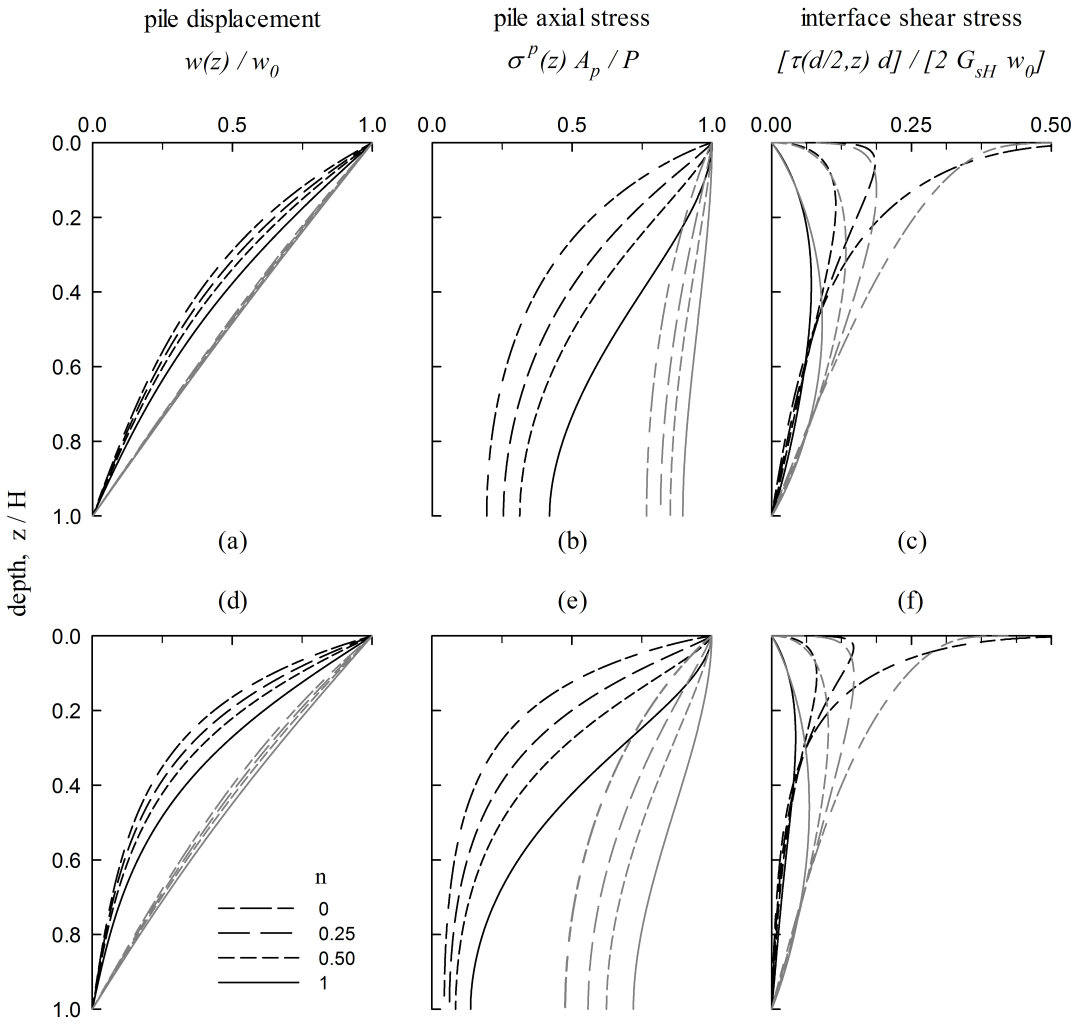

FIGURE 8 Profiles of pile displacement, vertical pile normal stresses and shear stresses at the pile-soil interface for different geometries of piles embedded in soils with zero stiffness at their surface ($b = 0$, Equation 2). The black curves refer to $E_p/E_{sH} = 100$ and the grey curves to $E_p/E_{sH} = 1000$. Sub-figures $(a)-(c)$ correspond to $L/d = 25$ and sub-figures $(d)-(f)$ to $L/d = 50$. Number of modes used $N = 1500$.

pile head and decrease with depth (stronger attenuation for longer piles). The effect of pile slenderness (L/d) on displacement attenuation becomes less significant with increasing pile-soil stiffness ratio (grey curves). Comparing Figures 7 (b) and 7 (e)it is evident that the effect of soil inhomogeneity (for the values of n examined) on axial stresses is minor. In addition, vertical shear stresses at the soil-pile interface (Figures 7 (c) and 7 (f)) increase with depth until they attain a maximum value. Beyond that depth, normalised τ's decrease monotonically with depth. The depth of shear stress maxima depends on L/d, E_p/E_{sH} and n, while maximum values decrease with L/d (Figures 7 (c) and 7 (f)). Soft soils ($E_p/E_sH = 100$: grey curves) generate higher maxima, while increasing degree of inhomogeneity (7 (f): $n = 1$) slightly decrease maxima and shift them to a greater depth.

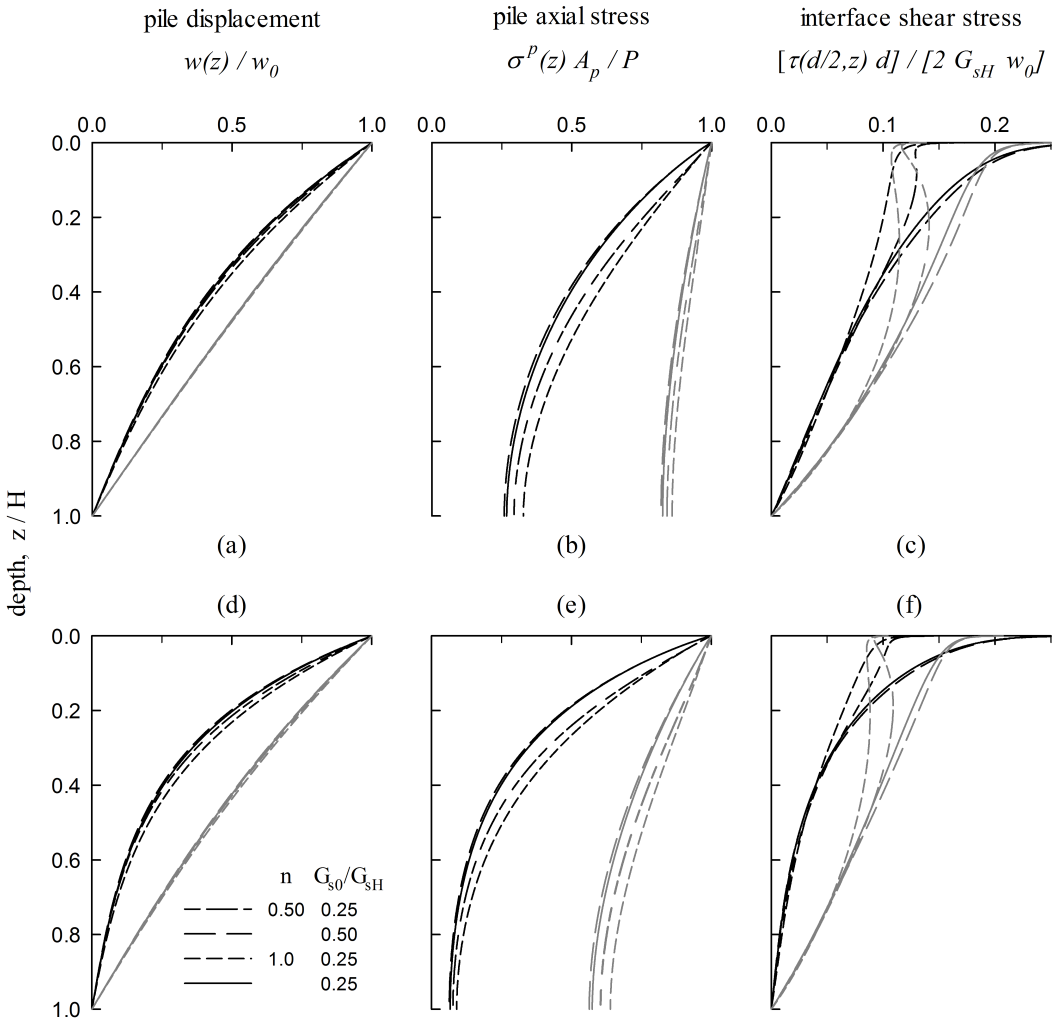

FIGURE 9 Profiles of pile displacement, normal pile axial stresses and sheer shear stresses at the pile-soil interface with depth for two selected geometries of piles embedded in soils with different degrees of inhomogeneity (i.e., n and b from Equations 1 and 2. The black curves refer to $E_p/E_{sH} = 100$ and the grey curves to $E_p/E_{sH} = 1000$. Sub-figures $(a) - (c)$ correspond to $L/d = 25$ and sub-figures $(d) - (f)$ to $L/d = 50$. Number of modes used $N = 1500$.

Additional numerical results are shown in Figures 8 and 9 for piles in soils with zero ($b = 0$) and finite stiffness ($b \neq 0$) at the soil surface, respectively. Figure 8 investigates the effect of soil inhomogeneity n on pile settlements, axial stresses and shear stresses at the soil-pile interface for two families of pile geometries ($L/d = 25$ and 50). It is shown that for given L/d and E_p/E_{sH} ratios the settlement attenuation with depth is stronger for piles in homogeneous soils ($E_p/E_s = E_p/E_{sH}$), and drops with increasing n (Figures 8 (a), 8 (d)). This is more pronounced for long piles ($L/d = 50$) and stiff soil ($E_p/E_{sH} = 100$) as shown in Figure 8 (d) (black curves). For softer soil ($E_p/E_{sH} = 1000$), as shown in Figures 8 (a) and 8 (d) (grey curves), piles exhibit a column-like behaviour and soil inhomogeneity becomes unimportant (all curves practically converge to a single one, especially for $L/d = 25$). Regarding the attenuation of pile axial stresses with depth, a trend similar to the settlement

attenuation is observed: for given L/d and E_p/E_{sH} ratios, stress attenuation is stronger for piles in homogeneous soils, and drops with increasing degree of inhomogeneity n (Figures 8 (b), 8 (e)). The effect of inhomogeneity diminishes for soft soils (grey curves). The behaviour of side friction is investigated in Figures 8 (c) and 8 (f): in presence of homogeneous soil shear stresses follow a monotonic reduction with depth, while for inhomogeneous soil exhibit the same trend as the one discussed previously with respect to Figures 7 (c) and 7 (f). All curves converge at depths approximately equal to $0.5L$ and $0.75L$ for stiff (black curves) and soft soils (grey curves), respectively.

Figure 9 investigates the effect of non-zero stiffness at the soil surface on normalised pile settlements w, stresses σ^p and shear tractions τ. While the behaviour of w's and σ^p's is similar to those depicted in Figures 7 and 8 , τ's behaviour for $b \neq 0$ is more similar to those developing in homogeneous soil. The latter is contrary to the case of zero surface stiffness (Figures 7 and 8), where shear reactions for $n \neq 1$ tend to zero at $z = 0$.

6 | DEPTH-DEPENDENT WINKLER MODULUS

The depth-dependent (actual) Winkler modulus $k(z)$ can be obtained by dividing the side friction (Equation 16) by the corresponding pile settlement (Equation 29):

$$k(z) = \frac{\pi\, d\, \tau_0(z)}{\mathrm{w}(z)} = \frac{2\,\pi \sum_{m=1}^{\infty} B_m\, s_m\, K_1(s_m)\, G_s(z)\, \Phi_m(z)}{\sum_{m=1}^{\infty} B_m\, K_0(s_m) \Phi_m(z)} \tag{44}$$

Results for the depth-dependent, normalized Winkler moduli $k(z)/G_{sH}$ are presented in Figures 10 , 11 and 12 . All plots refer to the soil-pile configurations (i.e., L/d's, E_p/E_{sH}'s, n's, G_{s0}/G_{sH}'s) analysed previously in Figures 7 , 8 and 9 .

As shown in Figure 10 $k(z)/G_{sH}$ increase parabolic- and linear-like with depth, respectively, attaining a maximum close to the tip for both stiff and soft soils ($E_p/E_{sH} = 1000$) and the majority of pile geometries ($L/d = 15, 25, 50$) examined. This trend is observed for very long piles ($L/d = 100$) in soft soil ($E_p/E_{sH} = 1000$). However, for $L/d = 100$ in stiff soil ($E_p/E_{sH} = 100$), $k(z)$ follows a trend similar to vertical shear reactions presented in Figures 7 (c), 7 (f), attaining a maximum at some depth. With increasing n the maximum drops in value and shifts downwards to a greater depth. Soft soil generates higher k's for all cases examined: slightly higher for long piles $L/d = 100$, which become gradually significantly higher with decreasing L/d. This behaviour is supressed with increasing soil inhomogeneity.

Figure 11 investigates the effect of soil inhomogeneity n on the Winkler modulus for two selected pile geometries $L/d = 15$ and 50. For depths down to approximately $0.5L$, moduli k behave similar to the vertical shear stresses shown in Figures 8 (c) and 8 (f). Beyond that depth, where all curves intersect, the trend is reversed. This threshold depth depends on E_p/E_{sH} and L/d, and shifts downwards withincreasing pile length and decreasing soil stiffness.

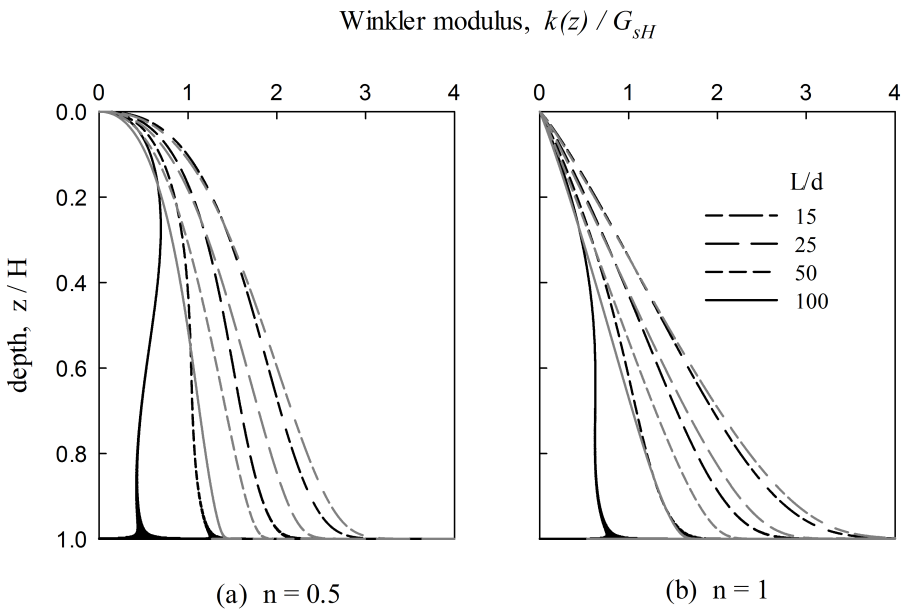

FIGURE 10 Variation of Winkler modulus with depth for different geometries of piles embedded in soils with zero stiffness at their surface ($b = 0$, Equation 2). The black curves refer to $E_p/E_{sH} = 100$ and the grey curves to $E_p/E_{sH} = 1000$. Number of modes used $N = 1500$.

Figure 12 investigates the effect of non-zero stiffness at the soil surface on $k(z)$ profiles. For all cases examined, k varies in an approximately linear manner with depth. For the special cases of $G_{s0}/G_{sH} = 0.50$ and stiff soil (black curves) Winkler moduli can be considered practically depth-independent.

7 | AVERAGE WINKLER MODULUS

Given the complexities associated with the variation of the Winkler modulus with depth, it is customary to adopt an average depth-independent, parameter to be used in engineering applications. In this light, $k(z)$ can be expressed as a function of the soil shear modulus $G_s(z)$ and a dimensionless, depth-independent, parameter δ

$$k(z) = \delta\, G_s(z) \tag{45}$$

which, upon substituting Equation 1, can be written as

$$k(z) = \delta\, G_{sr}\left[b + (1-b)\left(\frac{z}{z_r}\right)\right]^n \tag{46}$$

where $G_{sr} = G_s(z_r)$ is the soil shear modulus at a reference depth z_r. In light of this common approach, G_s and k attain the same variation with depth. To evaluate δ the pile head stiffnesses obtained from the proposed model are set equal to those obtained from a Winkler model. For a pile supported on vertical springs with stiffness obeying Equation 44, the pile head stiffness K is

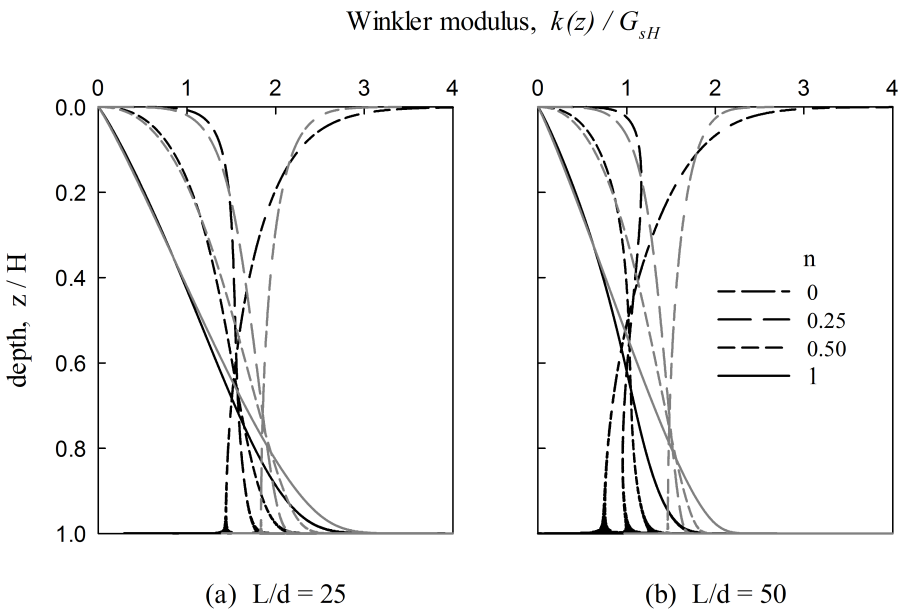

FIGURE 11 Variation of Winkler modulus with depth for two selected geometries of piles embedded in soils with zero stiffness at their surface ($b = 0$, Equation 2). The black curves refer to $E_p/E_{sH} = 100$ and the grey curves to $E_p/E_{sH} = 1000$. Number of modes used $N = 1500$.

obtained as[23,30,63]:

$$K = b^{n/2} E_p A_p \lambda_r \frac{K_{\mu-1}(\chi_0) I_\mu(\chi_L) + I_{\mu-1}(\chi_0) K_\mu(\chi_L)}{K_\mu(\chi_0) I_\mu(\chi_L) - I_\mu(\chi_0) K_\mu(\chi_L)} \tag{47}$$

where μ is a parameter associated with the order of the Bessel functions $I()$ and $K()$:

$$\mu = \frac{1}{n+2} \tag{48}$$

Parameter λ_r is analogous to the familiar Winkler parameter λ[64] at depth z_r

$$\lambda_r = \left(\frac{k_r}{E_p A_p}\right)^{1/2} = \frac{1}{d}\left(\frac{2}{\pi(1+\nu_s)}\right)^{1/2}\left(\frac{E_p}{E_{sr}}\right)^{-1/2}\delta^{1/2} \tag{49}$$

where $E_s r$ stands for the soil Young's modulus at $z = z_r$. In Equation 47 χ_L and χ_0 are dimensionless parameters obtained from $\chi(z)$, shown below, for $z = L$ and $z = 0$, respectively:

$$\chi(z) = \frac{2\lambda_r z_r}{(1-b)(n+2)}\left[b + (1-b)\left(\frac{z}{z_r}\right)\right]^{(n+2)/2} \tag{50}$$

Note that for the case of a long pile ($\chi_L \gg 1$), Equation 47 takes the simpler from

$$K = b^{n/2} E_p A_p \lambda_r \frac{K_{\mu-1}(\chi_0)}{K_\mu(\chi_0)} \tag{51}$$

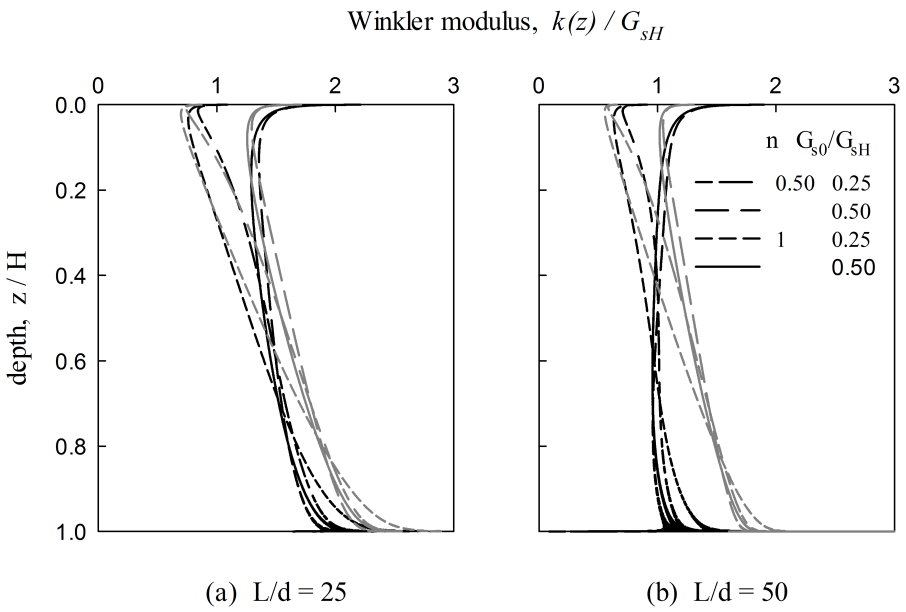

FIGURE 12 Variation of Winkler modulus with depth for two selected geometries of piles embedded in soils with different degrees of inhomogeneity (i.e., n and b from Equations 1 and 2. The black curves refer to $E_p/E_{sH} = 100$ and the grey curves to $E_p/E_{sH} = 1000$. Number of modes used $N = 1500$.

while for soils of zero stiffness at the surface ($b = 0$), Equation 47 reduces to

$$K = E_p A_p \lambda_r \left(\frac{n+1}{\lambda_r z_r}\right)^{n/(n+2)} \left[\Gamma\left(\frac{1}{n+2}\right)\right]^{-2} \left[\frac{\pi}{\sin\left(\frac{\pi}{n+2}\right)} + \frac{2 K_\mu(\chi_L)}{I_\mu(\chi_L)}\right] \tag{52}$$

where $\Gamma(\,)$ is the Euler Gamma function, and for $z_r = L$, $\chi_L = \chi(L) = (2\lambda_H L)/(n+2)$.

Note that for $n = 0$, the solution reduces to that of the solution of Mylonakis & Gazetas[65]. In this regard Equations (51) and (52) reduce to the following equations, respectively[65,27,28]:

$$K = E_p A_p \lambda \tag{53}$$

and

$$K = \frac{E_p A_p \lambda}{\tanh(\lambda L)} \tag{54}$$

To facilitate the use of the Winkler expressions presented in this section to evaluate the pile head stiffness, a simple flow-chart like graph (Figure A1) is provided in the Appendix.

Figure 13 presents the variation of δ ($= k/G_{sH}$) with pile slenderness L/d for soils with zero stiffness at surface, selected values of soil inhomogeneity and pile-soil stiffness ratios. Evidently, δ decreases with increasing L/d with the drop being stronger in soft soil. Further, with increasing n, δ attains higher values with the exception of stiff soil ($E_p/E_{sH} = 100$) where the trend is reversed beyond approximately $L/d = 60$. Overall, δ attains values in the range $1.5 \lesssim \delta \lesssim 4$. In the same figure δ's

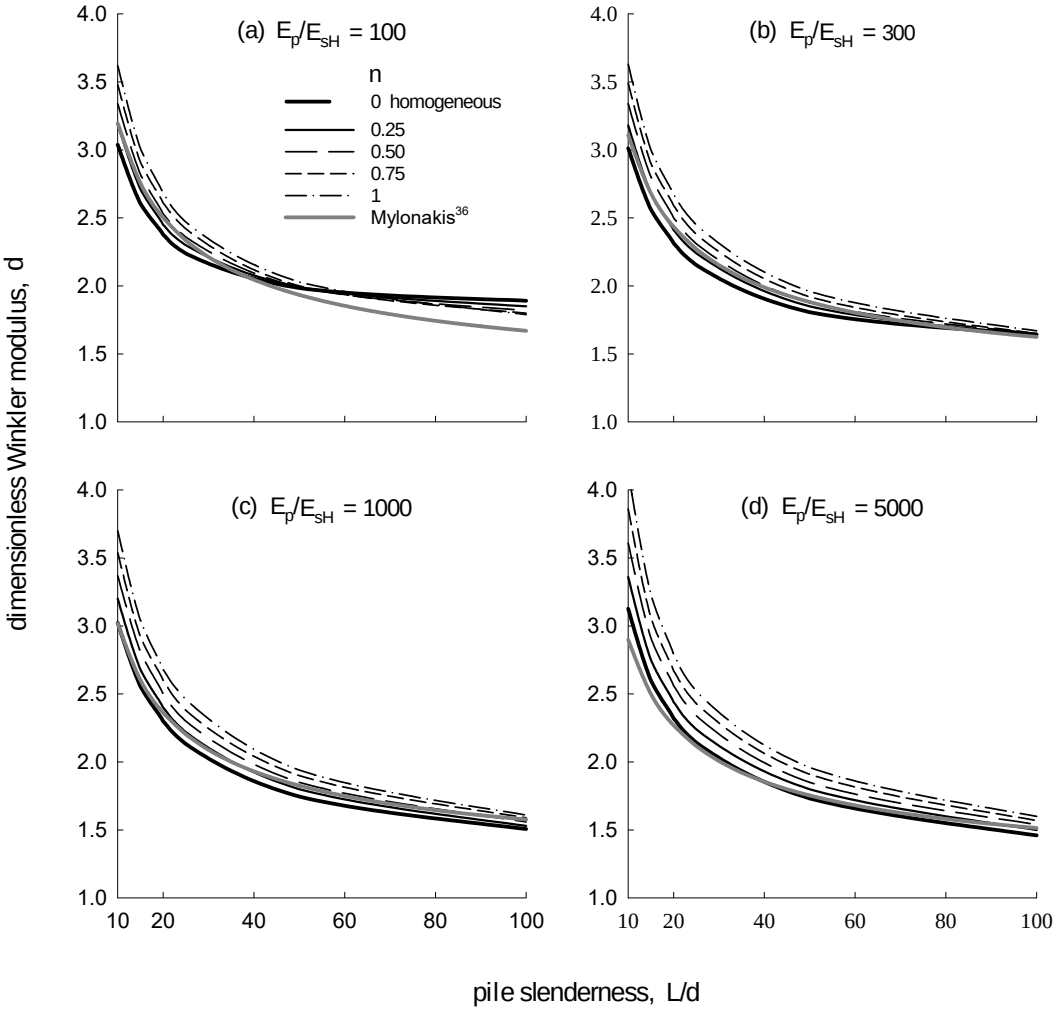

FIGURE 13 Dimensionless average Winkler modulus $\delta = k/G_{sH}$ to match pile head stiffness for selected values of the soil inhomogeneity parameter n and pile-soil stiffness ratios for a soil with zero stiffness at its surface ($b = 0$, Equation 2). Comparison against δ values obtained from the fitted formula of Mylonakis[36].

are compared against values obtained from a regression formula proposed by Mylonakis[36] for homogeneous soil:

$$\delta = 1.3\left(\frac{E_p}{E_{sH}}\right)^{-1/40}\left[1 + 7\left(\frac{L}{d}\right)^{-0.6}\right] \tag{55}$$

where E_s in the original expression is replaced with E_{sH}. It should be noticed that using a different Young's modulus, such as the average value of E_s along the pile, will have a negligible influence on the results given the minor dependence of δ on E_p/E_s. Equation 47 follows closer the results for homogeneous soil, with the agreement improving with increasing E_p/E_{sH}.

Figure 14 investigates the performance of the Winkler model in predicting pile head stiffness (Equation 47) using δ from Equation 55. Comparisons with results from the proposed model, for soils with zero stiffness at the surface, confirm the good performance of the Winkler model for a wide range of n and E_p/E_{sH} values. Remarkably, the accuracy of the predictions seem to improve with increasing levels of inhomogeneity.

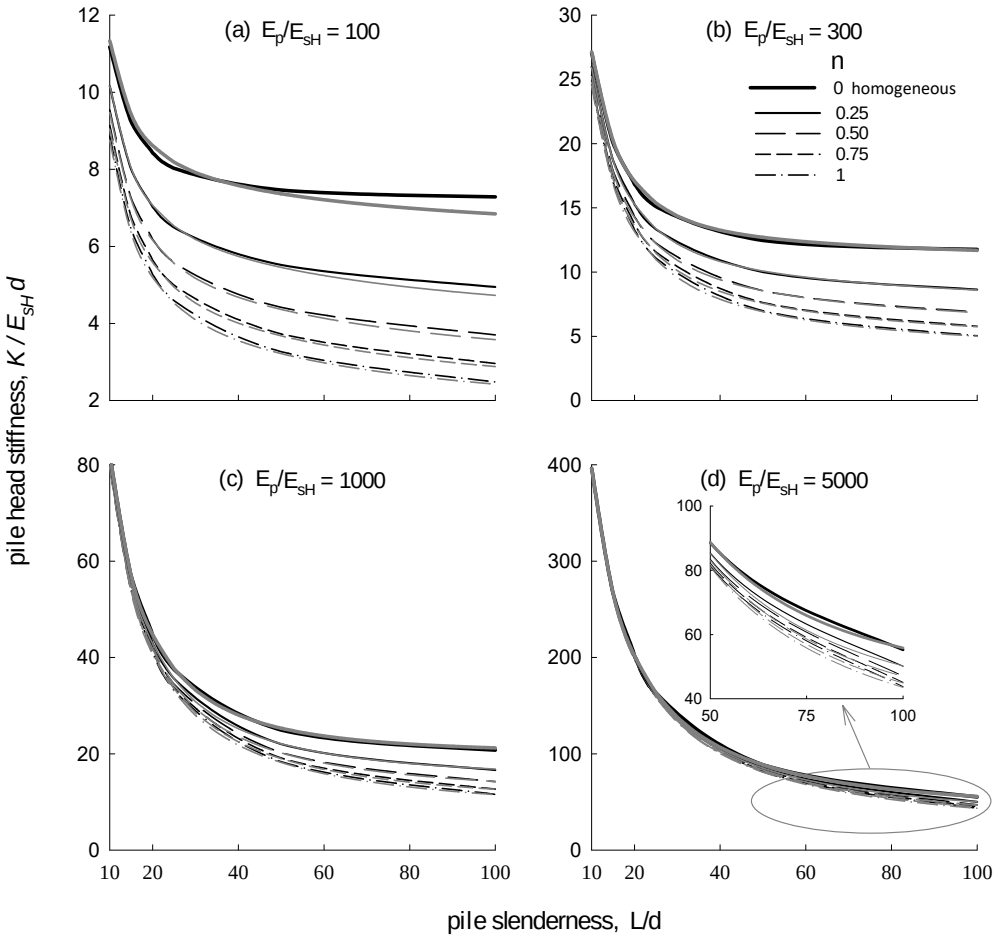

FIGURE 14 Variation of pile head stiffness with pile slenderness for selected values of the inhomogeneity parameter n and pile-soil stiffness ratio E_p/E_{sH}, for a soil with zero stiffness at its surface ($b = 0$, Equation 2). Comparison of the proposed model (Equation 43) illustrated with black curves against results based on the fitted formula of Mylonakis[36] (Equations 55 and 52) illustrated with grey curves. Number of modes used $N = 500$.

8 | CONCLUSIONS

This study focuses on: (i) the derivation of an elastic analytical solution of the Tajimi-type and a Winkler model to investigate the static behaviour of axially-loaded end-bearing piles in vertically inhomogeneous soil; (ii) pile head stiffness for different inhomogeneous soils; (iii) average, depth-independent, Winkler moduli (in terms of the dimensionless subgrade reaction moduli δ) to calculate pile head stiffness using a simple Winkler model. The main conclusions are summarised below:

1 The novel expansion of the second derivative of the soil modes Φ'' in the equilibrium equation of the pile over the vertical coordinate in terms of the soil modes Φ, is key to formulating the analytical solution.

2 A large number of modes (10^2 to 10^3) must be employed in the realm of this method to capture pile-soil interaction effects in a satisfactory manner, contrary to structural dynamics where the first mode often governs response. Further, higher modes are influenced more from inhomogeneity, exhibiting stronger peaks and troughs with increasing n.

3 Comparisons of pile head stiffness against results from finite element analyses indicate a very good performance across a variety of pile-soil configurations (L/d = 15 to 100; E_p/E_{sH} = 100 to 1000), with maximum deviation from the rigorous solution of about 7% (for long, soft piles). Overall, using 10^3 modes, the discrepancy does not exceed 2% or so.

4 For soils with zero stiffness at the surface, pile stiffness drops with increasing pile slenderness; the decrease being stronger for small L/d's. The effect of inhomogeneity is stronger for low pile-soil stiffness contrast. Also, higher n values correspond to lower head stiffness for a given L/d. For non-zero stiffness at the soil surface, pile head stiffness increases with increasing G_{s0}/G_{sH} (this trend is stronger for stiff soil) with higher values corresponding to lower n's. Overall, soft soils supress the influence of inhomogeneity on pile response.

5 Elastic pile settlement attenuation with depth is weaker with increasing soil inhomogeneity. This trend is more pronounced for long piles in stiff soil, while in soft soil piles exhibit a column-like behaviour and inhomogeneity effects become unimportant.

6 Axial pile stresses were calculated by integrating the side friction along the pile. This approach avoids spurious undulations associated with the differentiation of pile settlement with depth, even when a small number of modes is employed. Normalised axial stresses attain maximum values at the pile head, decrease with depth (the rate of decrease being stronger for long and soft piles), while seem practically unaffected by soil inhomogeneity.

7 Side friction increases with depth and attains a maximum prior to decrease monotonically. Depths for maxima depend on L/d, E_p/E_{sH} and increase with increasing inhomogeneity n. Further, maxima decrease with L/d and n and increase with E_p/E_{sH}. In homogeneous soil, side friction decreases monotonically with depth and all curves converge at depths of approximately $0.5L$ and $0.75L$ for stiff and soft soils, respectively.

8 A Winkler solution for pile head stiffness in inhomogeneous soils was revisited. Two families of depth-independent normalised Winkler moduli δ to predict pile head stiffness were explored: the first was derived by matching the pile head stiffness obtained from the proposed formulation with that from a Winkler solution for inhomogeneous soil, while the second was a fitted formula adopted from an existing solution for uniform soil. The performance of the Winkler solution in conjunction with the fitted formula for δ was satisfactory for a broad range of pile-soil configurations and can be used in practice.

9 For inhomogeneous soils with zero stiffness at the surface ($b = 0$), pile-soil stiffness ratios ($100 \leq E_p/E_{sH} \leq 5000$) and pile slenderness ratios ($10 \leq L/d \leq 100$), Winkler parameter δ ($= k/G_{sH}$) is primarily affected by L/d, not by E_p/E_{sH}, and attains values in the range $1.5 \lesssim \delta \lesssim 4$.

Finally, it is fair to mention that in the herein reported analysis the effects of stress induced soil softening as well as buckling, are not explicitly addressed, while the solution is limited by the presence of a rigid bearing layer. Relaxing these assumptions lies beyond the scope of this work, however will be considered for future work.

Likewise the critical pile length, beyond which the pile behaves as infinitely long is not discussed as this length exceeds most pile lengths commonly encountered in engineering applications[65].

How to cite this article: Anoyatis G., G. Mylonakis, and A. Tsikas (20XX), An analytical continuum model for axially-loaded end-bearing piles in inhomogeneous soil, *International Journal for Numerical and Analytical Methods in Geomechanics*, *20XX;XX:XX–XX*.

APPENDIX

A QUICK GUIDE TO CALCULATE PILE HEAD STIFFNESS K

Figure A1 simple flow-chart like graph is provided to evaluate pile head stiffness $\boldsymbol{K}$ using the Winkler expressions provided in the main text.

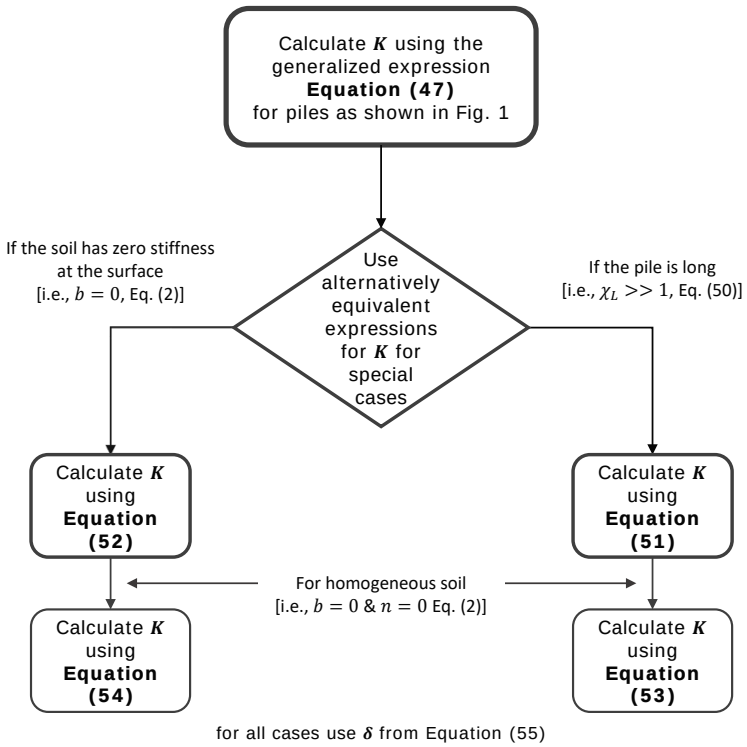

FIGURE A1 Simple guide to calculate pile head stiffness K using Winkler expressions.

References

1. Ottaviani M. Three-dimensional finite element analysis of vertically loaded pile groups. *Géotechnique.* 1975;25(2):159–174.

2. Pressley JS, Poulos HG. Finite element analysis of mechanisms of pile group behaviour. *International journal for numerical and analytical methods in geomechanics.* 1986;10(2):213–221.

3. Trochanis AM, Bielak J, Christiano P. Three-dimensional nonlinear study of piles. *Journal of Geotechnical Engineering.* 1991;117(3):429–447.

4. Syngros K. *Seismic response of piles and pile-supported bridge piers evaluated through case histories.* PhD Thesis: City University of New York; 2004.

5. Eid HT, Shehada AA. Estimating the Elastic Settlement of Piled Foundations on Rock. *International Journal of Geomechanics.* 2013;15(3):04014059.

6. Davis EH, Poulos HG. The use of elastic theory for settlement prediction under three-dimensional conditions. *Géotechnique.* 1968;18(1):67–91.

7. Banerjee PK, Davies TG. The behaviour of axially and laterally loaded single piles embedded in nonhomogeneous soils. *Géotechnique.* 1978;28(3):309–326.

8. Poulos HG. Settlement of single piles in non homogeneous soil. 1978;.

9. Kaynia AM, Kausel E. Dynamics of piles and pile groups in layered soil media. *Soil Dynamics and Earthquake Engineering.* 1991;10(8):386–401.

10. Chin JT, Chow YK, Poulos HG. Numerical analysis of axially loaded vertical piles and pile groups. *Computers and Geotechnics.* 1990;9(4):273–290.

11. Matos Filho R, Mendonça AV, Pva JB. Static boundary element analysis of piles submitted to horizontal and vertical loads. *Engineering analysis with boundary elements.* 2005;29(3):195–203.

12. Seed HB, Reese LC. The action of soft clay along friction piles. *American Society of Civil Engineers Transactions.* 1955;.

13. Coyle HM, Reese LC. Load transfer for axially loaded piles in clay. *Journal of the Soil Mechanics and Foundations Division.* 1966;92(2):1–26.

14. Kraft Jr LM, Ray RP, Kagawa T. Theoretical tz curves. *Journal of Geotechnical and Geoenvironmental Engineering.* 1981;107(ASCE 16653).

15. Li L, Li J, Sun D, Gong W. Semi-analytical approach for time-dependent load–settlement response of a jacked pile in clay strata. *Canadian Geotechnical Journal.* 2017;54(12):1682–1692.

16. Armaleh S, Desai CS. Load-deformation response of axially loaded piles. *Journal of geotechnical engineering.* 1987;113(12):1483–1500.

17. Mandolini A, Viggiani C. Settlement of piled foundations. *Géotechnique.* 1997;47(4):791–816.

18. Chin JT, Poulos HG. Axially loaded vertical piles and pile groups in layered soil. *International journal for numerical and analytical methods in geomechanics.* 1991;15(7):497–511.

19. Padrón LA, Aznárez JJ, Maeso O. Dynamic analysis of piled foundations in stratified soils by a BEM–FEM model. *Soil Dynamics and Earthquake Engineering.* 2008;28(5):333–346.

20. Shadlou M, Bhattacharya S. Dynamic stiffness of pile in a layered elastic continuum. *Géotechnique.* 2014;64(4):303.

21. Ai ZY, Chen YF, Jiang XB. Behavior of laterally and vertically loaded piles in multi-layered transversely isotropic soils. *Applied Mathematical Modelling.* 2017;51:561–573.

22. Poulos HG, Davis EH. *Pile foundation analysis and design*. No. Monograph1980.

23. Scott RF. *Foundation analysis*. Englewood Cliffs, NJ : Prentice-Hall; 1981.

24. Poulos HG. Pile behaviour-theory and application. *Géotechnique.* 1989;39(3):365–415.

25. Pender MJ. Aseismic pile foundation design analysis. *Bulletin of the New Zealand National Society for Earthquake Engineering.* 1993;26(1):49–160.

26. Randolph MF. Science and empiricism in pile foundation design. *Géotechnique.* 2003;53(10):847–876.

27. Salgado R. *The engineering of foundations*. McGraw-Hill New York; 2008.

28. Fleming K, Weltman A, Randolph M, Elson K. *Piling engineering*. CRC press; 2014.

29. Viggiani C, Mandolini A, Russo G. *Piles and pile foundations*. CRC Press; 2014.

30. Guo WD. *Theory and practice of pile foundations*. CRC press; 2012.

31. Randolph MF, Wroth CP. Analysis of deformation of vertically loaded piles. *Journal of Geotechnical and Geoenvironmental Engineering.* 1978;104(ASCE 14262).

32. Baguelin F, Frank R. Theoretical studies of piles using the finite element method. In: Thomas Telford Publishing 1980 (pp. 83–91).

33. Nogami T, Novák M. Soil-pile interaction in vertical vibration. *Earthquake Engineering & Structural Dynamics.* 1976;4(3):277–293.

34. Akiyoshi T. Soil-pile interaction in vertical vibration induced through a frictional interface. *Earthquake Engineering & Structural Dynamics.* 1982;10(1):135–148.

35. Pak RYS, Ji F. Rational mechanics of axial soil-pile interaction. *Journal of Engineering Mechanics.* 1993;119(4):813–832.

36. Mylonakis G. Winkler modulus for axially loaded piles. *Géotechnique.* 2001;51(5):455–462.

37. Anoyatis G, Di Laora R, Mylonakis G. Axial kinematic response of end-bearing piles to P waves. *International Journal for Numerical and Analytical Methods in Geomechanics.* 2013;37(17):2877–2896.

38. Matsuo H, Ohara S. Lateral earth pressure and stability of quay walls during earthquakes. In: :165–181Science Council of Japan Tokyo-Kyoto, Japan; 1960.

39. Tajimi H. Dynamic analysis of a structure embedded in an elastic stratum. In: :53–69; 1969.

40. Westergaard HM. A problem of elasticity suggested by a problem in soil mechanics: soft material reinforced by numerous strong horizontal sheets. *Contributions to the mechanics of solids, Stephen Timoshenko 60th anniversary volume.* 1938;:268–277.

41. Nogami T, Novak M. Resistance of soil to a horizontally vibrating pile. *Earthquake Engineering & Structural Dynamics.* 1977;5(3):249–261.

42. Novak M, Nogami T. Soil-pile interaction in horizontal vibration. *Earthquake Engineering & Structural Dynamics.* 1977;5(3):263–281.

43. Saitoh M. Fixed-head pile bending by kinematic interaction and criteria for its minimization at optimal pile radius. *Journal of Geotechnical and Geoenvironmental Engineering.* 2005;131(10):1243–1251.

44. Anoyatis G, Mylonakis G. Dynamic Winkler modulus for axially loaded piles. *Géotechnique.* 2012;62(6):521.

45. Anoyatis G, Mylonakis G, Lemnitzer A. Soil reaction to lateral harmonic pile motion. *Soil Dynamics and Earthquake Engineering.* 2016;87:164–179.

46. Anoyatis G, Lemnitzer A. Dynamic pile impedances for laterally–loaded piles using improved Tajimi and Winkler formulations. *Soil Dynamics and Earthquake Engineering.* 2017;92:279–297.

47. Younan AH, Veletsos AS. Dynamic response of flexible retaining walls. *Earthquake engineering & structural dynamics.* 2000;29(12):1815–1844.

48. Veletsos AS, Younan AH. Dynamic response of cantilever retaining walls. *Journal of Geotechnical and Geoenvironmental Engineering*. 1997;123(2):161–172.

49. Anoyatis G, Myloankis G. Novel Tajimi models for static and dynamic soil-pile Interaction. In: G. De Roeck G. Lombaert G. Muller, ed. *8th International Conference on Structural Dynamics*, :170–177EURODYN; 2011; Leuven, Belgium.

50. Novak M, Sheta M. Approximate approach to contact effects of piles. In: ASCE; 1980.

51. Veletsos AS, Dotson KW. Vertical and torsional vibration of foundations in inhomogeneous media. *Journal of geotechnical engineering*. 1988;114(9):1002–1021.

52. El-Sharnouby B, Novak M. Stiffness constants and interaction factors for vertical response of pile groups. *Canadian geotechnical journal.* 1990;27(6):813–822.

53. Di Laora R, Rovithis El. Kinematic bending of fixed-head piles in nonhomogeneous soil. *Journal of Geotechnical and Geoenvironmental Engineering*. 2014;141(4):04014126.

54. Guo WD. Vertically Loaded Single Piles in Gibson Soil. *Journal of Geotechnical and Geoenvironmental Engineering*. 2000;126(2):189-193.

55. Gibson RE. Some results concerning displacements and stresses in a non-homogeneous elastic half-space. *Géotechnique*. 1967;17(1):58–67.

56. Anoyatis G. *Contribution to kinematic and inertial analysis of piles by analytical and experimental methods*. PhD Thesis: University of Patras, GR; 2013.

57. Davis HF. *Fourier series and orthogonal functions*. Courier Corporation; 1989.

58. Abramowitz M, Stegun IA. *Handbook of mathematical functions: with formulas, graphs, and mathematical tables*. Courier Corporation; 1964.

59. ANSYS-10.0 . Finite element commercial software. Canonsburg, PA, US.

60. Novak M, El Sharnouby B. Stiffness Constants of Single Piles. *Journal of Geotechnical Engineering*. 1983;109(7):961-974.

61. Banerjee PK, Davies TG. Analysis of pile groups embedded in Gibson soil. In: :381-3869th International Conference of Soil Mechanics and Foundation Engineering; 1977; Tokyo, Japan.

62. Guo WD, Randolph MF. Rationality of load transfer approach for pile analysis. *Computers and Geotechnics*. 1998;23(1):85 - 112.

63. Crispin J, Leahy C, Mylonakis G. Winkler Model for Axially-Loaded Piles in Inhomogeneous Soil. *Géotechnique Letters.* 2018;8(4):1-25.

64. Anoyatis G, Di Laora R, Mandolini A, Mylonakis G. Kinematic response of single piles for different boundary conditions: analytical solutions and normalization schemes. *Soil Dynamics and Earthquake Engineering.* 2013;44:183–195.

65. Gazetas G, Mylonakis G. Settlement and additional internal forces of grouped piles in layered soil. *Géotechnique.* 1998;48.

AUTHOR BIOGRAPHY

George Anoyatis is a Senior Lecturer in Civil Engineering at the University of the West of England, UWE in Bristol, UK. Before moving to Bristol he joined the Structural-Geotechnical Research Group of the Civil and Environmental Engineering Department at the University of California, Irvine (UCI) as a Post Doctoral Scholar. He holds PhD and MSc degrees from the University of Patras, GR and a Diploma degree from the National Technical University of Athens (NTUA), GR. He specializes on dynamics of pile foundations with emphasis on the development of closed-form elastodynamic solutions. Dr. Anoyatis is a member of various professional societies and serves as a reviewer for ten national and international journals.

George Mylonakis is a Professor and the Head of the Earthquake & Geotechnical Engineering Research Group at the University of Bristol (UoB), UK. He holds a 5-year Diploma Degree in Civil Engineering from NTUA, GR and a PhD in Geotechnical & Earthquake Engineering from SUNY-Buffalo. He is a recipient of the Prakash International Research Award (2002). He has served as Guest Editor and/or Editorial Board Member in 5 International Journals. He has been Principal Investigator in more than 20 funded research projects and his publications have attracted over 2500 citations by independent researchers. He holds academic appointments at UoB, UPatras and UCLA.

Aggelos Tsikas is the Managing Director (Research Engineering in Complex Energy Projects) at Monogram AS, Oslo, Norway. He holds MSc and PhD degrees in Mathematics from the Carnegie Mellon University, US as well as an MSc in Structural and Computational Mechanics from the same institution. He obtained a Diploma degree in Civil Engineering from the National Technical University of Athens (NTUA) where he served as a Post-Doctoral Research Associate upon completion of his doctoral studies. Dr Tsikas is the recipient of awards for excellence in mathematical skills. His research interests are within the areas of computational science and engineering and continuum mechanics.